Wood Science and Technology 31 (1997) 225–234 © Springer-Verlag 1997

Theory of X-ray measurement of microfibril angle in wood

Part 2. The diffraction diagram
X-ray diffraction by materials with fibre type symmetry

I. D. Cave

Summary A diffraction intensity function for material bodies composed of arrays of crystalline fibres such as occurs with the cellulose of wood has been derived. It is implied in the analysis that the crystalline fibres making up the body have fibre symmetry- that there is a tendency for groups of fibres to have one set of crystal axes parallel while in the orthogonal direction the axes assume a low degree of order. It is further assumed that the patterns of the angular arrangement of the fibre groups relative to one axis of the body is independent of the direction about that axis. These conditions are believed to be compatible with the cellulosic structure found in wood. Thus it becomes possible to calculate the expected diffraction intensity profiles of realistic (and therefore complex) models of wood. This has aided the interpretation of the reflections from the (040) crystal planes of cellulose which are contaminated by low level reflections from other crystal planes, and it has been found that it might be possible by conjoint analysis of the paratropic (002) reflections and the diatropic (040) reflections to measure the complete cell wall planar microfibril angle distribution and the shape of the cell wall cross-section.

Introduction

The degree and nature of the orientation of the long, straight, very stiff and crystalline cellulose microfibrils in natural fibres has long been known to be a major determinant of the stiffness of the fibre. For example, Spark et al. (1958) attributed a 30:1 variation in stiffness in sisal fibres (delignified) to a 10°–50° range of mean microfibril angle.

The mean microfibril angle in the S2 layer of the secondary cell walls of softwood has been used as a key parameter in understanding the mechanical behaviour of whole wood and separated fibres, (Meylan and Probine 1969; Page et al. 1977). Further, closer modelling of softwood structure has indicated the importance that the relatively minor quantities of cellulose of transverse orientation in the cell wall has in determining shrinkage behaviour, (Barber 1968).

To date there has been no convenient way to determine an average microfibril angle distribution of a test specimen. In fact, except for the use of X-ray diffraction there is no convenient method to measure even an average mean microfibril angle of the S2 layers of softwood tracheids, (Meylan 1967).

Received 5 October 1995

I. D. Cave
RD2 Upper Moutere, Nelson, New Zealand 7152

This work is supported by the New Zealand Foundation for Research Science and Technology under contract # UOC 401

The possibility that X-ray diffraction can be used to measure the complete microfibril angle distribution of the cell wall has arisen following an analysis of the condition for reflection of materials with fibre type symmetry, (Cave 1997). The present paper takes those results to calculate the diffraction intensity profiles of model wood tissue. From the insights gained it becomes possible to devise a way by which complete microfibril angle distributions might be measured.

Discussion

While cellulose crystals have very small cross-sections composed of a regular array of about 100 or so β-1,4 linked glucosidic chains they are relatively large compared with the wavelength of X-rays so that the interaction of such beams with the atoms of the crystals produce diffraction effects. The diffraction patterns of single crystals contain information that can be used to establish spatial relationships between the atoms of the crystal, whereas in large assemblages of independent crystals, such as occur in wood, diffraction patterns can yield recoverable information about the alignment of the crystals. For cellulose we are interested in the patterns of alignment of the longitudinal axes of the microfibrils (**b** crystal axes), that tend to be aligned in well defined groups. On average there is no preferred alignment of the **a** and **c** crystal axes, thereby bestowing the property of fibre symmetry on the cellulose system in wood, a property that is central to this argument.

The cross-section of the crystallites of cellulose in the higher plants can be estimated from figures provided by Preston (1974) as approximately 8.0 nm × 3.9 nm. In comparison the wavelength of the Cu K_α X-rays usually used in this work is 0.154 nm. Typically the earlywood of *Pinus radiata* has a cellulose volume ratio of 0.45 and average tracheid diameter of 34μm with a cell wall thickness of 2–3μm, (Cave 1976). This means that an optimal X-ray specimen of 1.5 mm thickness presents about 900 tracheids to a beam of 0.75 mm diameter with more than 3×10^9 independent cellulose crystallites capable of reflecting radiation.

Under these conditions the resultant diffracted beam consists of the superposition of a large number of independent identical reflected waves of random phase difference (Pain, 1983) so that the energy of the radiation scattered into an element of solid angle is proportional to the number of crystallites reflecting into that element.

The position the reflected beam in terms of the orientation of the microfibril axis within the specimen has been derived in Cave (1997).

In the simplest terms crystalline microfibrils may be regarded as regular reflectors with the angle of reflection equal to the angle of incidence, as in an optical mirror, except that reflections occur only at specific angles, (Bragg angles, denoted by θ) dependent on the spacing between the planes giving rise to the reflection. With the use of a crystal diffractometer, reflections from a single set of crystallographic planes may be examined at one time by setting the angle between the incident beam and the axis of the detector to 2θ and rotating the specimen about an axis set at an angle θ to the incident beam, in the plane of the source and the detector, to record the variation of the reflection intensity with scan angle ψ, (see Fig. 1 for the layout of the apparatus and the definitions of quantities). The position of a reflected beam is specified by the Bragg angle θ and the azimuth ψ at which reflections occur. The angle ψ has been shown to be a function of the two angles α and μ defining the microfibril direction relative to the specimen coordinates and the direction of the reflection plane normal relative to the microfibril

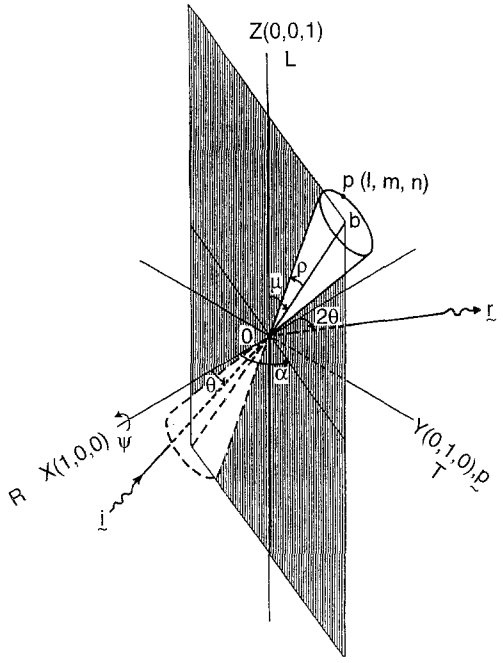

Fig. 1. Geometry of the specimen and X-ray diffraction system: X,Y,Z laboratory co-ordinates, L,R,T specimen co-ordinates; the specimen is mounted at O and is rotated about axis, OX; **i** is the incident X-ray beam; **r** is the diffracted beam; **p** is the reflection condition vector; **b** is the longitudinal microfibril axis; α is the cell wall element plane angle, measured relative to the specimen L-R plane; μ is the microfibril angle; ρ is the angle between the microfibril axis and the reflecting plane normal; θ is the Bragg angle for reflection. (taken from Cave, 1997)

axis, the angle ρ. An element of solid angle accepting reflected radiation can therefore be effectively specified by θ and $\psi \pm d\psi$, where $\psi \equiv \psi(\rho, \alpha, \mu)$.

Diffraction energy

Thus the energy dE, entering the aperture of the detector may be written, $I_{\rho,\alpha,\mu}(\psi)d\psi$, where $I_{\rho,\alpha,\mu(\psi)}$ is the intensity at ψ, arising from the number of reflectors, dN, that meet the condition for reflection during the rotation from $\psi - d\psi$ to $\psi + d\psi$.

That is,

$$dE = I_{\rho,\alpha,\mu}(\psi)d\psi \propto dN.\Delta(\rho, \alpha, \mu), \tag{1}$$

where, $\Delta(\rho, \alpha, \mu) = 1$ if the condition for reflection, is met and zero if not.

There are four solutions to $\psi(\rho, \alpha, \mu)$, for each set (ρ, α, μ) provided that,

$$\cos \rho / R \leq 1, \tag{2}$$

where,

$$R = (\sin^2 \mu \sin^2 \alpha + \cos^2 \mu)^{1/2} \quad 0 \leq \alpha < 2\pi \text{ and } -\pi/2 \leq \mu \leq \pi/2.$$

Relation (2) represents the condition for reflection. Reflections are forbidden when it is not met.

The four solutions are,

$$\begin{aligned} \psi_1 &= 2n\pi - \Theta - \eta, \\ \psi_2 &= 2n\pi - \Theta + \eta, \\ \psi_3 &= (2n-1)\pi - \Theta - \eta, \\ \psi_4 &= (2n-1)\pi - \Theta + \eta, \quad n = 1, 2, 3 \cdots \end{aligned} \tag{3}$$

where,

$$\Theta = \cot^{-1}(\tan\mu \sin\alpha), \quad -\pi/2 \leq \Theta \leq \pi/2 \tag{4}$$

and,

$$\eta = \cos^{-1}(\cos\rho/R) \quad 0 \leq \eta \leq \pi/2. \tag{5}$$

Microfibril angle distribution

From this point it is assumed that dN can be written,

$$dN = F(\alpha).f(\mu)d\mu. \tag{6}$$

$f(\mu)$ is a continuous function representing the frequency distribution of microfibril angle in a planar element of cell wall with orientation specified by the azimuth angle α.

$F(\alpha)$ serves either as a continuous function defining the thickness of planar cell wall elements tangential to the radial orientation α if the average cell representing the whole specimen can be regarded as having a continuous generator of cross-section, or discontinuous if the average cell has some form of polygonal cross-section.

With dN structured in this way it is implied that the microfibril angle distribution is identical in every cell wall element.

Diffraction intensity function

Setting $d\psi = \varepsilon$, a suitably small fixed number, we can write the intensity function for a range of μ centred about μ' in a planar cell wall element of orientation α, using (1) and (6) as,

$$I_{\rho,\alpha,\mu}(\psi) = \mathbf{I}_\rho \cdot \frac{1}{\varepsilon}F(\alpha) \cdot \int_{\mu'-\Delta\mu}^{\mu'+\Delta\mu} f(\mu)d\mu.\Delta(\rho,\alpha,\mu), \tag{7}$$

where,

$$\Delta\mu = \left(\frac{\partial\mu}{\partial\psi}\right)_{\rho,\alpha} \varepsilon,$$

and $\mathbf{I}_\rho$, the constant of proportionality is determined by the characteristics of the cellulose unit cell and the size of the crystallites.

We may now sum the energies in unit steps of ψ over α, μ and the four solutions. Thus, the intensity function for the complete representative cell is,

$$I_\rho(\psi) = \mathbf{I}_\rho. \sum_{s=1}^{4} \sum_{\alpha=0}^{2\pi} \sum_{\mu'=-\pi/2}^{\pi/2} \frac{1}{\varepsilon}F(\alpha). \int_{\mu'-\Delta\mu}^{\mu'+\Delta\mu} f(\mu)d\mu.\Delta(\rho,\alpha,\mu), \tag{8}$$

where s indexes the four solutions of ψ.

This result is an extension of that given by Prud'homme and Noah (1975) for cells of circular cross-section. From it we may calculate X-ray intensity profiles of model cells comprised of cell walls with a general microfibril angle distribution $f(\mu)$ and any cell cross-section defined by $F(\alpha)$, and for reflections from any set of crystallographic planes.

Diffraction intensity profiles

Reference is made in the following discussion to X-ray diffraction profiles of model microfibril distributions calculated on the basis of eqn. 8. Attention is confined to cell cross-sections that are either uniformly circular or square. The circular case is obtained by taking $F(\alpha) =$ constant in the range $0 \leq \alpha < 2\pi$, while square cell profiles are generated by taking
$F(\alpha) =$ constant when $\alpha = 0, \pi/2, \pi, 3\pi/2$, and zero for all other values.

There are a number of special cases of some interest.

1. The diatropic (040) planes[1] of cellulose ($2\theta = 34.5°$), produce a potentially useable scan of moderate intensity. In this case $\rho = 0°$ and so the condition for reflection is met only if $R = 1$. $R = 1$ only when $\alpha = 90°, 270°$, with $\eta = 0°$ and so ψ is simply $90° \pm \mu$, and $270° \pm \mu$. In Eq. (7) therefore, $|\alpha|$ is single valued, and $(\partial\mu/\partial\alpha)_{\rho,\alpha} = 1$, so that the intensity function $I_{\rho,\alpha,\mu}(\psi)$ directly mirrors $f_\mu(\mu)$.

In a complete cell,

$$I_\rho(\psi) = \mathbf{I}_\rho[f(90° - \mu) + f(90° + \mu) + f(270° - \mu) + f(270° + \mu)].$$

In some circumstances this does mean that the (040) intensity profile provides a direct measure of the microfibril angle distribution in the S2 layer in particular, as has been noted elsewhere, (Cave 1966; El-osta et al. 1973). However, if the range of μ includes values less than zero or greater than 90° then $f(90° + \mu)$ overlaps $f(90° - \mu)$ etc. and $I_\rho(\psi)$ does not strictly reflect $f(\mu)$.

It is to be expected that overlap always occurs for the microfibrils of the S1 and S3 layers (see for instance Kataoka, et al. 1992) but it may also occur for S2 layers with steep mean microfibril angle (Meylan, pers. comm.). Figure 2 illustrates the point. The normal error function of Fig. 2a is chosen to represent the microfibril distribution of an S2 layer of moderate mean microfibril angle (20° running in a Z helix, say) but with rather wide dispersion, (standard deviation 11°) so that there is a significant number of microfibrils with negative microfibril angles in a S helix. The resulting intensity profile, $I_\rho(\psi)$, for the (040) reflection is shown in Fig. 2b. The mean value of μ is clearly defined by the peak in $I_\rho(\psi)$ but only the outer flank of the intensity profile indicates the true dispersion of the microfibril angle distribution.

2. For the very strong paratropic (002) planes, ($2\theta = 22.6°$), $\rho = 90°$. There can be no cell wall azimuths that have forbidden reflections. η is constant and equal to 90°. However if $\alpha = 90°$ and 270° only, $I_{\rho,\alpha,\mu}(\psi)$ again mirrors $f(\mu)$, and in the tangential wall components of a perfectly square cell,

$$I_\rho(\psi) = \mathbf{I}_\rho[f(\mu) + f(-\mu) + f(180° - \mu) + f(180° + \mu)].$$

[1]The Meyer and Misch(1937) interpretation of the unit cell of cellulose is used to label the crystallographic planes

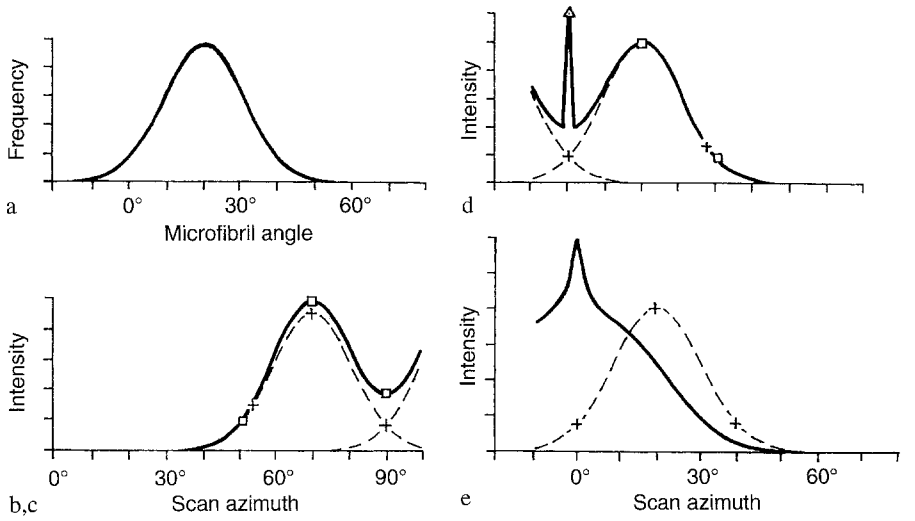

Fig. 2a–e. X-ray diffraction diagrams for (002) and pure (040) reflections; **(a)** Microfibril angle distribution in cell wall element plane; Gaussian, with mean angle = 20°, s.d. = 11° **(b)–(e)** diffraction diagrams for the cellulose distribution of **(a)**; **(b)** (040) reflections, square cell cross-section; □ tangential walls, + contributing microfibril distribution, **(c)** (040) reflections, circular cell cross-section; **(d)** (002) reflections, square cell cross-section; □ tangential walls, Δ radial walls, + contrib. mfibril. distr; **(e)** (002) reflections, circular cell cross-section. + contributing microfibril distribution. All intensity scales of arbitrary magnitude

Again overlap may occur if the microfibril distribution includes both S and Z helices, (Fig. 2d).

In reality there are always values of α other than 90° and 270° present to some extent so that with non-diatropic planes ψ is no longer independent of the value of α and the peak value in $I_\rho(\psi)$ is shifted to values of ψ less than the value of μ for which $f(\mu)$ peaks and the shape of $I_\rho(\psi)$ is not identical with $f(\mu)$. The case for a circular cross-section is illustrated in Fig. 2e.

3. The (040) reflection is contaminated by a number of weak reflections that have 2θ angles within 1° of the (040) 2θ angle of 34.5°. They have been tabulated in El-osta et al. (1973) and fall into three groups that can be characterised with the Miller indices (h3l), (h1l) and (h0l) and corresponding ρ values of 40.6°, 75.4° and 90°. The intensity profiles of these reflections are shown in Fig. 3a–d for the microfibril angle distribution given in Fig. 3a. The four non-degenerate solutions for $\psi(\rho, \alpha, \mu)$ in these cases lead to double peaks in the tangential cell wall profile and characteristic spikes at $\psi = 90° \pm \rho$ and $270° \pm \rho$ from the radial walls. The radial wall spikes are also obvious in the circular cell profile. The (h0l) profile is the same as that given for (002) in Fig. 2d–e.

Towards resolving a complete microfibril angle distribution.

From the foregoing it can be seen that both (040) and (002) reflections have some problems associated with their use for evaluating the microfibril distribution.

Prud'homme and Noah (1975) proposed that $f(\mu)$ could be recovered from $I_\rho(\psi)$ in (002) reflections if the cells were circular by fitting the circular cell version of Eq. 8 to the intensity scan, while El-osta et al. (1973) described a computerised numerical method to resolve a pure (040) profile from a measured (040) X-ray diffraction profile contaminated by (h3l), (h1l) and (h0l) reflections,

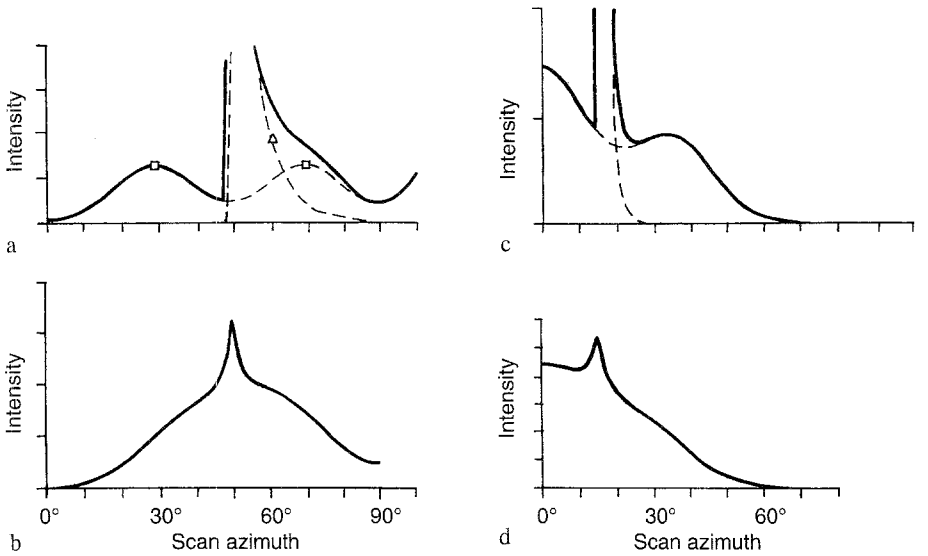

Fig. 3a–d. X-ray diffraction diagrams for (h3l) and (h1l) reflections for the cellulose distribution of Fig. 2a. **(a)** (h3l) reflections, square cell cross-section; □ tangential walls, Δ radial walls; **(b)** (h3l) reflections, circular cell cross-section; **(c)** (h1l) reflections, square cell cross-section; □ tangential walls, Δ radial walls; **(d)** (h1l) reflections, circular cell cross-section. All intensity scales of arbitrary magnitude

having assumed that the average cell cross-section was square, and then ascribed the resolved (040) profile directly to the S2 layer microfibril distribution.

Taking elements from both of these contributors, together with additional work on the condition for reflection and the intensity function, Cave (1997) speculated that the simultaneous use of both (040) and (002) reflections could be used to resolve $f(\mu)$ in a more general way and also provide an estimate of the function $F(\alpha)$ describing the average cell cross-sectional shape.

It is clear that comparison of (002) and (040) profiles of the same specimen would quickly reveal whether the average cell cross-section was likely to be square or not, since the pure (040) profile, in its outer parts anyway, is independent of the cross-section but for a low level of contamination by (h3l) in the region of $\psi = 90°–40.6°$, while the (002) will have a similar profile in the outer region of the major peak only if the average cell shape is square, Fig. 2.

Further, it is generally expected that $f(\mu)$ will be bimodal, with a major peak in the range $0 < \mu < 40°$ representing the cellulose in the S2 layer and a lesser peak in the range $50° < \mu < 90°$ representing the cellulose in the remaining cell wall layers. The presence of a significant S1/S3 peak will be shown by the presence of a corresponding minor peak or band raised above the background in the (002) profile. The (040) profile will also show radiation in the $50° < \mu < 90°$ region but some of this may have come from (h1l) and (h0l) reflections of the main $f(\mu)$ peak, in addition to the direct (040) radiation from the minor peak.

Cave (1997) proposed that the observed (040) scan might be used as a first approximation to $f(\mu)$ that could be run on a computation of the (002) profile and $F(\alpha)$ found by fitting to the observed (002) profile. The contaminant (h3l), (h1l) and (h0l) reflections could then be calculated and removed from the measured scan to derive a refined pure (004) profile. This new (040) profile would then be

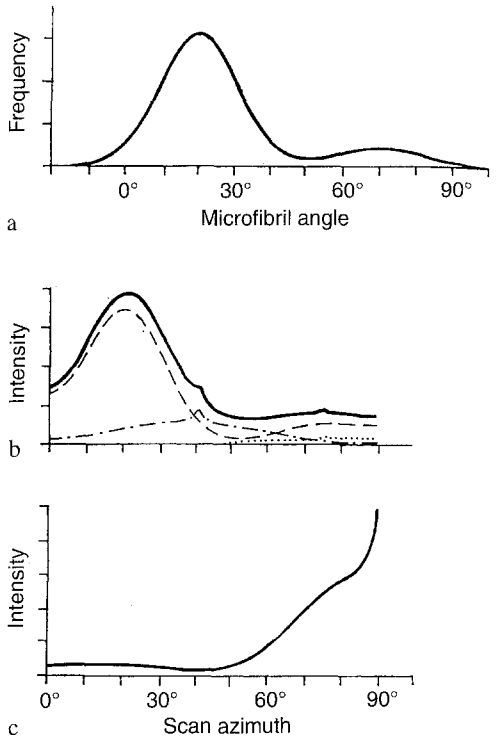

Fig. 4a–c. Diffraction diagram for a model of an earlywood trachied with circular cross-section. **(a)** Microfibril angle distribution in cell wall element plane; S2 layer vol. ratio = 0.86, S2 layer mfa distr. Gaussian, with mean angle = 20°, s.d. = 11°, S1/S3 layer mfa distr. Gaussian, with mean angle = 75°, s.d. = 12.5°. **(b)** Diffraction diagram for the cellulose distribution of (a) from (040) and contaminant planes. — Compound profile, -- pure (040) profile, ·-· (h3l) profile, scaling factor 0.17, ... (h1l) profile, scaling factor 0.05, (h0l) profile, scaling factor 0.01. **(c)** Diffraction diagram for the cellulose distribution of (a) from (002) planes

adopted as $f(\mu)$ and run back through the (002) computation to refine the estimate of $F(\alpha)$. The process could be iterated as desired up to the limits of resolution. However, in the light of the observations on overlap in the previous section, it may be preferrable to take the first approximation to $f(\mu)$ as a Gaussian with an estimated mean value and standard deviation based on the outer flanks of the (040) S2 peak plus a minor Gaussian suitably scaled to represent the S1/S3 layers if so indicated by the (002) scan.

The scaling factors for the (h3l), (h1l) and (h0l) profiles relative to the (040) are constants that depend on the deviation of the respective Bragg angles from the (040) value and the radial width, $d\theta$, of the scan arc which is a function of crystallite size and are multipliers for the proportionality constants $\mathbf{I}_\rho$ in these cases. Unfortunately the evaluation of the $\mathbf{I}_\rho$ appear to be problematic in cellulose (Preston, 1974) and so the scaling factors may have to be determined empirically.

The likely structure of a compound (040) X-ray scan of wood is revealed in Fig. 4, which portrays the overall computed profile and its constituents for a model wood cell with circular cross-section. The model represents a typical earlywood tissue of New Zealand grown *Pinus radiata* in which 86% of the cellulose is to be found in an S2 layer, with a mean microfibril angle in the range 15° to 30°, and the remainder of the cellulose, of the S1/S3 layers, in a hoop binding with a mean microfibril angle of 70° and standard deviation 12.5° (Cave 1976).

There are few published (040) profiles of wood available for comparison. However El-osta et al. (1973) in their Fig. 3c have provided one that will suffice for this purpose. It is from an earlywood specimen of Douglas-fir that has moderate to large mean microfibril angle with wide dispersion in the S2 layer.

Accordingly the *Pinus radiata* model, Fig. 4a, has been assigned an S2 layer microfibril angle distribution of Gaussian form with mean value 20° and standard deviation 11° while the hoop has mean value 75° and standard deviation 12.5°.

In order to correspond with the slightly different geometry of the X-ray system used by El-osta et al. (1973) the intensity functions in Fig. 4 are phase shifted by 90°.

Comparing the scans of the three specimens with widely differing S2 layer mean angles illustrated by El-osta et al. (1973), Fig. 5, it is apparent that the (h3l) planes make a significant contribution to the scan set at $2\theta = 34.5°$. In each, a small peak occurs about $\psi = 40.6°$ corresponding to the position of the (h3l) radial wall spike. There is also a small invariant peak about $\psi = 75.4°$ and again at $\psi = 90°$ perhaps. However it is not so clear that these correspond with the (h1l) and (h0l) plane reflections since it is certain that some of the radiation in this region arises from the (040) reflections of the S1/S3 layers.

The scaling factors of the (h3l), (h1l) and (h0l) reflections relative to the amplitude of the S2 (040) which were used to produce Fig. 4 were obtained merely by inspection and are roughly 0.17, 0.05, 0.01 respectively. The effect of (h3l) has been deliberately exaggerated to make the point that it, at the least, is an important contaminant of the (040) profile. This result further compromises any assertion that an unrefined (040) profile will lead to a direct measure of the microfibril distribution in the S2 layer.

The (002) profile for the same model is given in Fig. 4c.

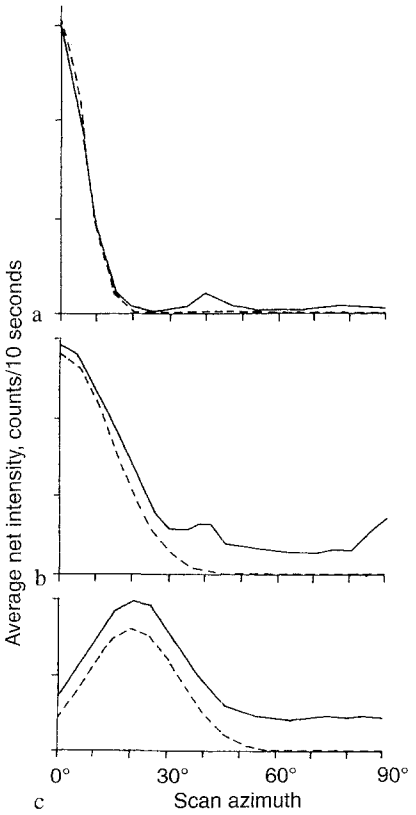

Fig. 5a–c Representative (040) diffraction profiles from El-osta et al. (1973). Early wood specimens with S2 mean microfibril angle of (**a**) about 8°; (**b**) about 17°; (**c**) about 27°. Reproduced with permission

Conclusion

An expression for the intensity of an X-ray beam diffracted from wood tissue has been developed with a view to using X-ray diffraction profiles to determine a complete cellulose microfibril angle distribution in the wood cell wall.

It is based on recent work on the condition for reflection and the relationship between crystallite orientation and the diffracted beam position, for materials with fibre type symmetry, (Cave 1997). It applies to the reflections from any set of crystal planes and is capable of predicting the shape of the diffraction profile formed from the most complex cellulosic structures of wood.

X-ray diagrams of model wood structures calculated using this expression demonstrate the influence that different features of the wood cell wall have on the diagrams of the differing crystal planes of cellulose and this information is of help in the interpretation of X-ray diagrams of wood, and particularly the (040) reflections which are contaminated by other weaker reflections.

Given that the angular distribution of the cellulose microfibrils in a planar cell wall element is independent of the position of the element on the cell wall circumference, it has been shown that the differing characteristics of paratropic and diatropic reflections might be exploited by conjoint analysis of, say, (002) and (040) diffraction profiles to find the average cellulose microfibril angle distribution of the cell wall and the average cross-sectional profile of the cells.

References

Barber, N. F. 1968: A theoretical model of shrinking wood. Holzforschung. 22: 97–103

Cave, I. D. 1976: Modelling the structure of the softwood cell wall for computation of mechanical properties. Wood Sci. Technol. 10, 19–28

Cave, I. D. 1997: X-ray Measurement of Microfibril Angle. Part 1: The Condition for Reflection. Wood Sci. Technol. (in press)

Kataoka, Y.; Saiki H.; Fujita M. 1992: Arrangement and Supperposition of Cellulose Microfibrils in the Secondary Walls of Coniferous Tracheids. Mokuzai Gakkaishi. 38: 327–355

El-osta, M.; Lotfy M.; Kellog, R. M.; Foschi, R. O.; Butters, R. G. 1973: A Direct X-Ray Technique for Measuring Microfibril Angle. Wood and Fiber. 5: 118–128

Meyer, K. H.; Misch, H. 1937: Positions des atomes dans le nouveau modèle spatial de la cellulose. Helv. Chem. Acta. 20: 232–244

Meylan, B. A. 1967: Measurement of microfibril angle in *Pinus radiata* by X-ray diffraction. Forest Prod. J. 17: 51–58

Meylan, B. A.; Probine, M. C. 1969: Microfibril angle as a parameter in timber quality assessment. Forest Prod. J. 19: 30–34

Page, D. H.; El-Hosseiny, F.; Winkler, K.; Lancaster, A. P. S. 1977: Elastic modulus of single wood pulp fibers. Tappi. 60: 114–117

Pain, H. J. 1983: The Physics of Vibrations and Waves. 3rd ed. John Wiley and Sons Ltd.

Preston, R. D.; Cronshaw, J. 1958: Constitution of the fibrillar and non-fibrillar components of the walls of *Valonia ventricosa*. Nature 181: 248–250

Preston, R. D. 1974: The Physical Biology of Plant Cell Walls. London: Chapman and Hall Ltd.

Prud'homme, R. E.; Noah, J. 1975: Determination of Fibril Angle Distribution in Wood Fibers: A comparison between the X-ray diffraction and the polarized microscope methods. Wood and Fiber. 6: 282–289

Spark, L. C.; Darnborough, G.; Preston, R. D. 1958: Structure and Mechanical Properties of Vegetable Fibres. II A Microextensometer for the automatic recording of load-extension curves for single fibrous cells. J. Text. Inst. 49: T309